

Multi-source thermal model describing multi-region structure of transverse momentum spectra of identified particles and parameter dynamics of system evolution in relativistic collisions

Jia-Yu Chen^{1,*}, Mai-Ying Duan^{1,†}, Fu-Hu Liu^{1,‡}, Khusniddin K. Olimov^{2,3,§}

¹*Institute of Theoretical Physics, State Key Laboratory of Quantum Optics and Quantum Optics Devices & Collaborative Innovation Center of Extreme Optics, Shanxi University, Taiyuan 030006, China*

²*Laboratory of High Energy Physics, Physical-Technical Institute of Uzbekistan Academy of Sciences, Chingiz Aytmatov Str. 2b, Tashkent 100084, Uzbekistan*

³*Department of Natural Sciences, National University of Science and Technology MISIS (NUST MISIS), Almaty Branch, Almaty 110105, Uzbekistan*

Abstract: In this article, the multi-region structure of transverse momentum (p_T) spectra of identified particles produced in relativistic collisions is studied by the multi-component standard distribution (the Boltzmann, Fermi-Dirac, or Bose-Einstein distribution) in the framework of a multi-source thermal model. Results are interpreted in the framework of string model phenomenology in which the multi-region of p_T spectra corresponds to the string hadronization in the cascade process of string breaking. The contributions of the string hadronizations from the first-, second-, and third- i.e. last-generations of string breakings mainly form high-, intermediate-, and low- p_T regions, respectively. From the high- to low- p_T regions, the extracted volume parameter increases rapidly, and temperature and flow velocity parameters decrease gradually. The multi-region of p_T spectra reflects the volume, temperature, and flow velocity dynamics of the system evolution. Due to the successful application of the multi-component standard distribution, this work reflects that the simple classical theory can still play a great role in the field of complex relativistic collisions.

Keywords: transverse momentum spectra; multi-region structure; multi-source thermal model; volume and temperature dynamics; system evolution

PACS: 12.40.Ee, 13.85.Hd, 24.10.Pa

1 Introduction

As physical quantities that can be measured in the experiments of relativistic hadron-hadron, hadron-nucleus, and nucleus-nucleus collisions, transverse momentum (p_T) spectra and other abundant data of identified hadrons can shed light on the mechanisms of particle production and characteristics of system evolution [1, 2, 3, 4]. In particular, the p_T spectra reflect the excitation degree of the system and the collective motion of produced particles. The excitation degree can be described by the thermal motion of particles, i.e. the temperature of the system or source. The collective motion can be described by the transverse flow velocity of particles or the transverse velocity of source's expansion, which causes the spectra to be blue-shifted. Generally, the contributions of thermal motion and flow effect are intertwined. If the temperature parameter is extracted from the data without excluding the contribution of flow

effect, we call it the effective temperature (T) which is not an intrinsic (or thermal) temperature. Generally, the kinetic freeze-out temperature (T_0) is the thermal temperature at the kinetic freeze-out stage of the system evolution, in which the flow effect is excluded in some way.

There are different methods to separate the contributions of thermal motion and flow effect. These methods include, but are not limited to, i) the method of blast-wave model [5, 6, 7, 8, 9] in which T_0 and average transverse flow velocity ($\langle\beta_T\rangle$) can be obtained from the experimental p_T spectra by using a probability density function in theory, ii) the method of applying the Lorentz-like transformation of p_T in theoretical p_T distribution [10, 11, 12, 13] so that the function of T is transformed into the function of T_0 and $\langle\beta_T\rangle$, and iii) the alternative method of intercept-slope [14, 15, 16, 17, 18] in which T_0 is obtained from the intercept of the linear relation of T versus m_0 , and $\langle\beta_T\rangle$ is obtained from the

*E-mail: 202012602001@email.sxu.edu.cn

†E-mail: duanmaiying@sxu.edu.cn

‡Corresponding author. E-mail: fuhuliu@163.com; fuhuliu@sxu.edu.cn

§Corresponding author. E-mail: khkolimov@gmail.com; kh.olimov@uzsci.net

slope of the linear relation of $\langle p_T \rangle$ versus $\langle m \rangle$, where $\langle p_T \rangle$ is the average p_T and $\langle m \rangle$ is the average energy (the average mass of the moving particles in the source rest frame). In the linear relation of T versus m_0 , $\langle \beta_T \rangle$ is related to, but not equal to, the slope [19, 20].

The method of extracting T_0 and $\langle \beta_T \rangle$ is not the main focus of this article. Instead, we focus our main attention on the general structure, i.e. the various regions [21, 22, 23], of p_T spectra. As we know, the p_T spectra cannot be fitted by a single function due to the emissions of multiple sources according to the multi-source thermal model [24, 25, 26, 27]. Naturally and at first, one may think that the p_T spectra can be divided into two regions: the high- and low- p_T regions. One may use different functions or distributions to fit the spectra in different p_T regions. For example, one may use the two-component function, the Hagedorn function or inverse power law from the quantum chromodynamics (QCD) calculus [28, 29, 30, 31] as the second component to fit the spectra in the high- p_T region, and the standard distribution (the Boltzmann, Fermi-Dirac, or Bose-Einstein distribution) from the Boltzmann-Gibbs statistics or the Tsallis distribution from the Tsallis statistics [32, 33, 34, 35] as the first component to fit the spectra in the low- p_T region due to different scenarios in particle production.

In the fit of two-component function, the spectra in the high- p_T region is regarded as the result of hard scattering process which drives the increase of the particle yield in high temperature region, and the spectra in the low- p_T region is considered as the result of soft excitation process which contributes to the low temperature region. If the two-component function fails to fit the p_T spectra, one may consider the three-component function in which the third, second, and first components correspond to the high-, intermediate-, and low- p_T regions, respectively, and the temperatures from the third, second, and first components reduce orderly. Indeed, sometimes, the p_T spectra have to be divided into three regions: the high-, intermediate-, and low- p_T regions. The multi-component function corresponds to the multi-region of p_T spectra, which is a natural result of the multi-source thermal model [24, 25, 26, 27].

As a statistical model, the multi-source thermal model [24, 25, 26, 27] does not provide the dynamic information of the system evolution due to the fact that the time order of particle production from different sources is not available in it, though various temperatures corresponding to different p_T regions can be obtained by using the same standard distribution or Tsallis statistics [32, 33, 34, 35]. The idea that the same distribution can be applied in different p_T regions is based on the similarity and universality that existed in relativistic collisions [36, 37, 38, 39, 40, 41, 42, 43]. It is necessary to note that the multi-source thermal

model [24, 25, 26, 27] is combined with other models such as the string model [44, 45, 46], and more abundant information related to the system evolution can be extracted from the p_T spectra.

In this article, we will study the method for describing the p_T spectra in the multi-source thermal model. Combining with the string model phenomenology, the idea and method for extracting the effective temperatures of various sources at different states of the system evolution are presented. As an application of the simple idea and method, we will study the p_T spectra in collisions at the Relativistic Heavy Ion Collider (RHIC) as an example. Naturally, the p_T spectra in collisions at other energies can be studied by the same idea and method. Although the Tsallis distribution can be widely used in the description of the p_T spectra, it is not suitable to describe the multi-region structure of the p_T spectra due to the fact that it trowels the structure. So, only the standard case will be studied by us to describe the multi-region structure.

The remainder of this article is structured as follows. The picture and formalism of the multi-source thermal model are described in Section 2. An application of multi-component standard distribution is given in Section 3. In Section 4, we give our summary and conclusions.

2 Formalism and method

According to the multi-source thermal model [24, 25, 26, 27], some emission sources are assumed to be formed in relativistic collisions. In the model, there are different particle-products which are originated from different kinds of sources, though the same or similar functions or distributions can be used to describe various particle-products and their sources. To understand the whole picture of the multi-source in detail, let us first introduce different sources of nuclear fragments and produced particles. The picture of multi-source results in the multi-region structure of transverse momentum spectra of nuclear fragments and produced particles, though the formation mechanisms of emission sources corresponding to the two kinds of products are different.

For nuclear fragments (such as a proton, neutron, deuteron, triton, helium, lithium, etc.) emitted mainly from the spectator region which is beyond the overlap area of projectile and target nuclei, the emission sources may be nucleons and nucleon clusters. For particles (such as π^\pm , K^\pm , and p which are light flavor particles, and J/ψ , $\psi(2S)$, and $\Upsilon(1S)$ which are heavy flavor particles) produced mainly in the participant zone that is in the overlap area, the emission sources may be quarks or partons. A few particles are produced in the spectator due to the cascade collisions between the par-

ticles produced in the participant zone and the nucleons of the spectator prefragment. Here, the spectators are the fragments/free nucleons that are produced after the deexcitation of the spectator prefragment. The number of particles produced in such cascade decay depends on the collision energy and size of participant/spectator zone. The emission sources of the particles produced in the spectator may be nucleons and/or other particles, which is similar to the particle production in statistical bootstrap model of hadronic matter [47, 48, 49].

Because of the relative motion, there is a friction between the spectator and participant. The contact layer between the spectator and participant may get more heat to stay in a high degree of excitation. The other part in the spectator may get less heat to stay in a low degree of excitation. The contact layer is a hot source, and the other part is a cold source, of nuclear fragments. That is to say that, the nuclear fragments are emitted with two-temperature. Considering that the transfer of friction heat takes time, the nuclear fragments from the hot source are emitted earlier than those from the cold source.

Not only for the cold source, but also for the hot source, one may use the standard or Tsallis distribution to describe the p_T spectra of nuclear fragments. The total result is the sum of the contributions of two components (the cold or first component and the hot or second component) with different temperatures (T_1 and T_2) and fractions (k and $1 - k$), where k is the fraction of cold reservoir. Generally, $T_1 < T_2$ and $k > 1 - k$, however, the relative size of k and $1 - k$ is not absolute. If the spectator is small enough, the transfer time of friction heat is negligible, we have $T_1 \approx T_2$. Thus, the spectator fragments are simultaneously emitted with a single temperature in case of a small spectator prefragment.

For particles produced in violent collisions in the participant region, the temperatures of various sources are different due to different timescales of source formations and particle productions. The particles in the high- p_T region are produced earlier than those in the low- p_T region. The source temperature of particles in the high- p_T region is higher than that in the low- p_T region. That is, we may use the standard or Tsallis distribution of two-component (two-temperature) to describe the p_T spectra of particles. The first component with a low temperature T_1 and a fraction k contributes in the low- p_T region, and the second component with a high temperature T_2 and a fraction $1 - k$ contributes in the high- p_T region. We have $T_1 < T_2$ if the particles in the high- p_T region are produced earlier than those in the low- p_T region, or $T_1 \approx T_2$ if the particles in both the high- and low- p_T regions are produced at the nearly same time.

In terms of string model phenomenology [44, 45, 46], many strings are formed due to parton interactions in

relativistic collisions. These strings will undergo the processes of hadronization and breaking. The particles in the high- p_T region are produced in the hadronization process from the first-generation string. If the first-generation string does not undergo the hadronization process, it will undergo the breaking process and more second-generation strings are formed. In the two-component distribution, the particles in the low- p_T region are produced in the hadronization process from the second-generation string.

In the case of using the three-component distribution, the first component describes the particles in the low- p_T region which is contributed by the source with a low temperature T_1 and a fraction k_1 from the hadronization of the third-generation string. The second (third) component describes the particles in the intermediate- p_T (high- p_T) region which is contributed by the source with an intermediate (high) temperature T_2 (T_3) and a fraction k_2 ($k_3 = 1 - k_1 - k_2$) from the hadronization of the second-generation (first-generation) string, where the hadronization of the first-generation string contributes in the high- p_T region. Generally, $T_1 < T_2 < T_3$ and $k_1 > k_2 > k_3 = 1 - k_1 - k_2$.

Although the multi-source thermal model is a static thermodynamical and statistical model, the dynamical evolution of source temperature can be described by the model in terms of the above idea from the p_T spectra. Comparing with the data in different experimental conditions, the dependence of temperature with collision energy, event centrality, nuclear size, particle rapidity, particle mass, and quark mass can be obtained. The behavior of the temperature dependence can be used to study the mechanisms of particle production and characteristics of system evolution.

Let us examine the i -th component in the multi-component distribution. To study the p_T spectra from the most classic theoretical consideration, we only use here the standard distribution in the formalism representation. According to ref. [9], one has the invariant yield of the particle momentum (p) distribution to be

$$\begin{aligned} E \frac{d^3 N}{d^3 p} \Big|_i &= \frac{1}{2\pi p_T} \frac{d^2 N}{dy dp_T} \Big|_i \\ &= \frac{gV_i}{(2\pi)^3} E \left[\exp \left(\frac{E - \mu}{T_i} \right) + S \right]^{-1}, \quad (1) \end{aligned}$$

where $E = \sqrt{p^2 + m_0^2} = \sqrt{p_T^2 + m_0^2} \cosh y$ is the energy, m_0 is the rest mass, y is the rapidity, $g = 2s + 1$ is the spin degeneracy factor, s is the spin quantum number, and μ is the chemical potential of the considered particle; N is the number of identified particles and V_i is the volume (normalization constant) of the source or system at the temperature T_i (free parameter); while $S = 0, 1$, and -1 correspond to the Boltzmann, Fermi-Dirac, and Bose-Einstein distributions, respectively. The density

function of momenta is

$$\left. \frac{dN}{dp} \right|_i = \frac{gV_i}{(2\pi)^3} 4\pi p^2 \left[\exp \left(\frac{\sqrt{p^2 + m_0^2} - \mu}{T_i} \right) + S \right]^{-1} \quad (2)$$

which is normalized to N , where $\sqrt{p^2 + m_0^2}$ replaces E to show the dependence on momentum p clearly.

The unit-density function of p_T and the rapidity y is

$$\left. \frac{d^2 N}{dy dp_T} \right|_i = \frac{gV_i}{(2\pi)^2} p_T \sqrt{p_T^2 + m_0^2} \cosh y \times \left[\exp \left(\frac{\sqrt{p_T^2 + m_0^2} \cosh y - \mu}{T_i} \right) + S \right]^{-1}, \quad (3)$$

where $\sqrt{p_T^2 + m_0^2} \cosh y$ replaces E to show p_T and y clearly. The density function of p_T is

$$\left. \frac{dN}{dp_T} \right|_i = \frac{gV_i}{(2\pi)^2} p_T \sqrt{p_T^2 + m_0^2} \int_{y_{\min}}^{y_{\max}} \cosh y \times \left[\exp \left(\frac{\sqrt{p_T^2 + m_0^2} \cosh y - \mu}{T_i} \right) + S \right]^{-1} dy, \quad (4)$$

where y_{\min} and y_{\max} denote the minimum and maximum y respectively, in the considered mid- y bin. The density function of y is

$$\left. \frac{dN}{dy} \right|_i = \frac{gV_i}{(2\pi)^2} \cosh y \int_0^{p_{T \max}} p_T \sqrt{p_T^2 + m_0^2} \times \left[\exp \left(\frac{\sqrt{p_T^2 + m_0^2} \cosh y - \mu}{T_i} \right) + S \right]^{-1} dp_T, \quad (5)$$

where $p_{T \max}$ denotes the maximum p_T , which is infinity in mathematics and large enough (e.g. ~ 30 – 50 GeV/ c and above) when we fit the real data. The distribution range of y in Eq. (5) is infinity which is certainly beyond $[y_{\min}, y_{\max}]$ in Eq. (4).

Equation (5) is the distribution of y in the rest frame of the source. In fact, the longitudinal motions of a series of sources with different rapidities in the one-dimensional rapidity space have to be considered. The rapidity of the considered particle in the moving frame of the source is then revised to $y - Y$, where Y is the source rapidity. We have the new expression for the distribution of y to be

$$\left. \frac{dN}{dy} \right|_i = \frac{1}{Y_{\max} - Y_{\min}} \frac{gV_i}{(2\pi)^2} \int_{Y_{\min}}^{Y_{\max}} \cosh(y - Y) \times \int_0^{p_{T \max}} p_T \sqrt{p_T^2 + m_0^2} \times \left[\exp \left(\frac{\sqrt{p_T^2 + m_0^2} \cosh(y - Y) - \mu}{T_i} \right) + S \right]^{-1} dp_T dY, \quad (6)$$

where Y_{\min} and Y_{\max} denote the range of Y , which is mainly related to collision energy, but not the order i . Generally, $|Y_{\min}|$ and $|Y_{\max}|$ increase linearly with the increase of logarithmic collision energy [26].

Considering n components in total, we have the multi-component distribution or function to be

$$E \frac{d^3 N}{d^3 p} = \frac{1}{2\pi p_T} \frac{d^2 N}{dy dp_T} = \sum_{i=1}^n E \left. \frac{d^3 N}{d^3 p} \right|_i, \quad (7)$$

$$\frac{dN}{dp} = \sum_{i=1}^n \left. \frac{dN}{dp} \right|_i, \quad (8)$$

$$\frac{d^2 N}{dy dp_T} = \sum_{i=1}^n \left. \frac{d^2 N}{dy dp_T} \right|_i, \quad (9)$$

$$\frac{dN}{dp_T} = \sum_{i=1}^n \left. \frac{dN}{dp_T} \right|_i, \quad (10)$$

$$\frac{dN}{dy} = \sum_{i=1}^n \left. \frac{dN}{dy} \right|_i. \quad (11)$$

In terms of p_T density, as an example, the ratio of the contribution ($dN/dp_T|_i$) of the i -th component to that (dN/dp_T) of n components is defined as the fraction k_i of the i -th component, where k_i are the parameters that do not appear obviously in the above equations. Generally, the normalization gives $\sum_{i=1}^n k_i = 1$. In the fit of data, Eqs. (7)–(11) can be used in the right way according to different styles of data set.

The above discussions are applicable for other distributions such as the Tsallis distribution [32, 33, 34, 35]. In fact, for very large number of components, the standard case should result in the Tsallis distribution which has the invariant yield of particle distribution to be

$$E \left. \frac{d^3 N}{d^3 p} \right|_i = \frac{1}{2\pi p_T} \left. \frac{d^2 N}{dy dp_T} \right|_i = \frac{gV_i}{(2\pi)^3} E \left[1 + (q-1) \frac{E - \mu}{T_i} \right]^{-\frac{q}{q-1}}, \quad (12)$$

where q is the entropy index which describes the degree of non-equilibrium. Generally, $q > 1$, while $q = 1$ means an equilibrium. A larger q corresponds to a further deviation from the equilibrium. We have used the assumption of $E > \mu$. If $E < \mu$, $-E + \mu$ and $q/(q-1)$ should replace $E - \mu$ and $-q/(q-1)$ in the equation respectively.

The above discussions are also suitable for the Tsallis-standard (Tsallis form of standard) distribution

which describes the invariant yield of particle distribution as

$$\begin{aligned} E \frac{d^3 N}{d^3 p} \Big|_i &= \frac{1}{2\pi p_T} \frac{d^2 N}{dy dp_T} \Big|_i \\ &= \frac{gV_i}{(2\pi)^3} E \left\{ \left[1 + (q-1) \frac{E-\mu}{T_i} \right]^{\frac{q}{q-1}} + S \right\}^{-1}. \end{aligned} \quad (13)$$

Here, we have used again the assumption of $E > \mu$. If $E < \mu$, $-E + \mu$ and $-q/(q-1)$ should replace $E - \mu$ and $q/(q-1)$ in the equation respectively.

Besides the Tsallis and Tsallis-standard distributions, the q -dual and q -dual-standard distributions can also describe the p_T spectra in the region of 10 GeV/ c and above. According to ref. [50], the q -dual distribution represents the invariant particle yield in the form of

$$\begin{aligned} E \frac{d^3 N}{d^3 p} \Big|_i &= \frac{1}{2\pi p_T} \frac{d^2 N}{dy dp_T} \Big|_i \\ &= \frac{gV_i}{(2\pi)^3} E \sum_{n=0}^{\infty} (-S)^k \\ &\quad \times \left[1 + (n+1)(q-1) \frac{E-\mu}{T_i} \right]^{-\frac{q}{q-1}}, \end{aligned} \quad (14)$$

where n is an integer greater than or equal to 0. In a real fit, we can take the maximum value of n to be 10 based on our confirmatory calculation in which the contributions of the terms with $n > 10$ can be neglected. Analogously to the Tsallis-standard distribution, we write the q -dual-standard distribution as

$$\begin{aligned} E \frac{d^3 N}{d^3 p} \Big|_i &= \frac{1}{2\pi p_T} \frac{d^2 N}{dy dp_T} \Big|_i \\ &= \frac{gV_i}{(2\pi)^3} E \sum_{n=0}^{\infty} (-S)^k \\ &\quad \times \left\{ \left[1 + (n+1)(q-1) \frac{E-\mu}{T_i} \right]^{\frac{q}{q-1}} + S \right\}^{-1}. \end{aligned} \quad (15)$$

In the above equations, although μ can be regarded as a free parameter, it is nearly zero at relativistic energies [51, 52, 53, 54]. Therefore, the assumption of $E > \mu$ can be satisfied in general. In the fit, the main parameters are V_i and T_i , while $k_i = V_i / \sum V_i$ that is expressed as a function of V_i . Generally, at first, we use the first component to fit the spectra as wide as possible in low- p_T region. Then, we add the second component to fit the spectra as wide as possible in intermediate- p_T region. Finally, we add the third component to fit the spectra in high- p_T region. It should be noted that when the second component is included, the parameters of the first component should be fixed to the value found before.

However, due to the influence of two sets of parameters from the two components, the parameters of the first component will have some changes to obtain the minimum χ^2 . In the fit, the method of least squares is used to determine the best values of parameters, and the method of statistical simulation [55] is used to determine the uncertainties of parameters in our work. Compared with fitting three components simultaneously without fixing any parameters in advance, the stepwise fitting method used by us can give the results more quickly. Generally, the two fitting methods can get consistent values of parameters because we have obtained the minimum χ^2 to determine various parameters.

Our previous work [56] shows that the temperature parameter extracted from the standard distribution is lower than the one from the Tsallis distribution, and the temperature parameter extracted from the Tsallis distribution is lower than the one from the Tsallis-standard distribution. A two- or three-component standard distribution can be covered by the Tsallis distribution, and a two- or three-component Tsallis distribution can be covered by the Tsallis-standard distribution. Because the standard distribution is the most basic and classical distribution, we are inclined to use the standard distribution with multi-component in the fit of multi-region of p_T spectra. The multi-temperature is a description of various stages of the system evolution.

In the fit of standard distribution, we need a two- or three-component function. The fine structure of p_T spectra can be described by the two- or three-component standard distribution which results from the multi-source thermal model [24, 25, 26, 27]. Generally, the first component describes the spectra in low- p_T region which results from the hydrodynamic evolution of partons. The second component describes the spectra in intermediate- p_T region which originates from the coalescence and fragmentation of partons. Meanwhile, the third component describes the spectra in high- p_T region which derives from the hard-scattering of partons.

Because of the underlying participants or contributors being partons for the spectra in whole p_T region, the maximum energy density of partons determines common behavior and basic property of p_T spectra. If the multi-component standard distribution describes the fine structure of p_T spectra, the single distributions such as the Tsallis, Tsallis-standard, q -dual, and q -dual-standard distributions do not reveal the fine structure in wide p_T region. Although the mentioned single distributions with fewer parameters are more suitable for the fit, the multi-component standard distribution can be used to extract the volume and temperature dynamics of the system evolution.

Before fitting the p_T spectra using the multi-component standard distribution, we would like to point out that the temperature fluctuation is a way to explain

the origin of the nonextensive distributions of the Tsallis statistics. Because of the temperature fluctuation, the interactions among the different local sources or subsystems happen through the exchange of heat energy, and result in the couplings of entropy functions of various subsystems. As a result, the total entropy is the sum of entropies of subsystems plus entropies of the couplings.

These nonextensive distributions of the Tsallis statistics are related to the Boltzmann's factor by a continuous summation of the Boltzmann factor weighed by factors given by the Euler-Gamma function. Thus, one can expect that, for proton-proton collisions, adding a sufficiently high number of components would approximate the result to a Tsallis distribution. For nucleus-nucleus collisions, the distribution would be deformed, with the effects of the collective flow modifying the Euler-Gamma function.

As mentioned above, in the multi-component distribution, different components correspond to different mechanisms of particle production. Generally, the feed-down contributions of resonances are in the very low- p_T region [57], which is naturally considered by us in the first component and contributed by the third- i.e. the last-generation of string breakings. If the relative contributions of resonances are large, a small T_1 and a large k_1 will be obtained. On the contrary, a large T_1 and a small k_1 will be obtained if the relative contributions of resonances are small. Here, we emphasize that the first component describes the spectra in low- p_T region which results from the third-generation of string breakings.

3 Results and discussion

To study the temperature dynamics of the system evolution, we use the multi-component standard distribution in the framework of multi-source thermal model to analyze the spectra of various particles at different energies. As an example, we analyze the spectra of neutral pions (π^0) produced in collisions at the RHIC. Figure 1(a) shows the invariant yields, $(1/2\pi p_T N_{EV})d^2N/dydp_T$, of π^0 produced in mid-pseudorapidity ($|\eta| < 0.35$) in gold-gold (Au-Au) collisions in different centralities at the center-of-mass energy per nucleon pair $\sqrt{s_{NN}} = 200$ GeV, where N_{EV} denotes the number of events. The various symbols represent the experimental data measured by the PHENIX Collaboration [58]. The curves are our fits with the multi-component standard distribution. The samples for different centralities are re-scaled by different factors marked in the panel. Following Figure 1(a), the values of Data/Fit corresponding to the fits are shown in Figure 1(b). The values of normalization constants V_1 , V_2 , and V_3 , free parameters T_1 , T_2 , and T_3 , as well as χ^2 and number of degrees-of-freedom (ndof) are listed

in Table 1. One can see that the PHENIX data are well fitted by the multi-component standard distribution.

Figure 2(a) shows the invariant yields, $(1/2\pi p_T N_{EV})d^2N/dydp_T$, of π^0 produced in $|\eta| < 0.35$ in 0–10% copper-copper (Cu-Cu) collisions at $\sqrt{s_{NN}} = 200$ and 62.4 GeV. In addition, Figure 3(a) shows the invariant cross-sections, $Ed^3\sigma/d^3p$, of π^0 produced in $|\eta| < 0.35$ in proton-proton (pp) collisions at $\sqrt{s_{NN}} = 200$ and 62.4 GeV, where σ denotes the cross-section of π^0 production. The symbols represent the experimental data measured by the PHENIX Collaboration [59]. The solid curves are our fits by the multi-component standard distribution. At 200 GeV, three-component function provides better results. The contributions of the first, second, and third components corresponding to the third, second, and first generations of string breakings are represented by the dotted, dot-dashed, and dashed curves, respectively, to underline their particular roles in the formation of the spectra. At 62.4 GeV, the two-component function proves suitable. The roles of the first and second components are illustrated by the dotted and dashed curves, accordingly. Following Figures 2(a) and 3(a), the values of Data/Fit corresponding to the fits are shown in Figures 2(b) and 3(b) respectively. The values of parameters, χ^2 , and ndof are listed in Table 1, where the values of V_1 , V_2 , and V_3 for Figure 3 are obtained from the re-normalization from the cross-section to yield so that we may compare these parameters uniformly. One can see again that the PHENIX data are well-fitted by the multi-component standard distribution.

Although the Data/Fit ratios oscillate around the unity, this can be attributed to the statistics of the experimental data. In addition, there are structures in the ratio plots, with groups of adjacent points deviating from the unity in one or another direction. There is a special oscillation for Cu-Cu data around the transverse momentum of 8 GeV/ c , which is the place where the dominating component of the fit changes. Larger oscillation for pp data is caused by the small interaction volume which does not result in more equilibrium than large interaction volume. In our opinion, this behavior shows that the model describes approximately the data due to the fact that it is formally consistent with the experimental errors. In the end, the χ^2 /ndof values, on which the experimental errors of the data have a strong influence, are acceptable due to small χ^2 /ndof, though the fit quality in a few cases in Figures 2 and 3 is not very satisfactory due to high values of χ^2 /ndof. In general, the present fits are acceptable, though four-component function with 8 parameters is expected to possibly obtain a better fit.

From Figures 1(b)–3(b) and Table 1, one can see that the fitting result in nucleus-nucleus collisions is better than that in pp collisions. This is explained by the large

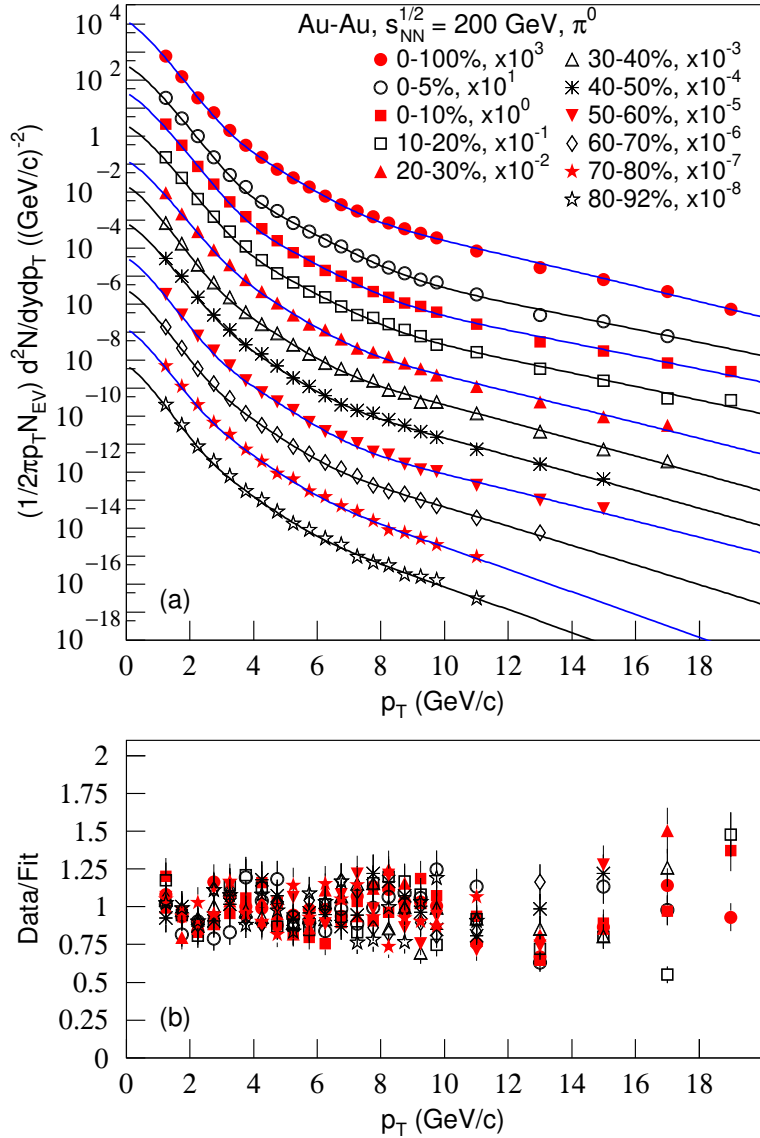


Fig. 1. (a) The invariant yields, $(1/2\pi p_T N_{EV})d^2N/dydp_T$, of π^0 produced in $|\eta| < 0.35$ in Au-Au collisions with different centralities at $\sqrt{s_{NN}} = 200$ GeV. The symbols represent the experimental data measured by the PHENIX Collaboration [58]. The curves are our fits by the multi-component standard distribution, Eqs. (1) and (7). (b) Values of Data/Fit corresponding to the fits in panel (a).

volume and then more equilibrium in nucleus-nucleus collisions. In the system with large volume, the thermodynamic equilibrium is easier to achieve. As a result, the standard distribution is more applicable.

From Table 1 one can see the tendencies of parameters. To see clearly, the dependences of V_1 , V_2 , and V_3 (upper panel), as well as T_1 , T_2 , and T_3 (lower panel), on the centrality C in 200 GeV Au-Au collisions are given in Figure 4. Meanwhile, the dependences of the free fitting parameters in different centrality classes (C) relative to the peripheral centrality class (80–92%), $(V_i - V_i|_{80-92\%})/V_i|_{80-92\%}$ (upper panel) and $(T_i - T_i|_{80-92\%})/T_i|_{80-92\%}$ (lower panel), on C in 200 GeV Au-Au collisions are displayed in Figure 5. As

marked in the panels, the different symbols represent different parameters. One can see that with the decrease of centrality from central to peripheral collisions, V_1 decreases significantly, V_2 has an increasing trend from central to semi-central collisions and a decreasing trend from semi-central to peripheral collisions, and V_3 fluctuates somehow and has no obvious increasing or decreasing trend. Meanwhile, with the decrease of centrality, T_1 decreases slightly, T_3 decreases significantly, and the decreasing degree of T_2 is between T_1 and T_3 .

At the same energy per nucleon pair, the parameters V_i decrease significantly and the parameters T_i decrease slightly from nucleus-nucleus to pp collisions in most cases. Although an increase appears from Au-Au

Table 1. Values of normalization constants V_1 , V_2 , and V_3 , free parameters T_1 , T_2 , and T_3 , as well as χ^2 and ndof corresponding to the solid curves in Figures 1–3, where the values of V_1 , V_2 , and V_3 for Figure 3 are obtained from the re-normalization from cross-section to yield so that we may compare them with those for Figures 1 and 2 uniformly.

Figure	Selection	V_1 (fm ³)	V_2 (fm ³)	V_3 (fm ³)	T_1 (MeV)	T_2 (MeV)	T_3 (MeV)	χ^2 /ndof
Figure 1	0–100%	15179.314 ± 1609.007	20.427 ± 1.626	0.005 ± 0.001	257.3 ± 3.3	545.5 ± 4.8	1440.0 ± 9.4	18/17
Au-Au	0–5%	37593.234 ± 4586.375	12.253 ± 1.225	0.003 ± 0.001	270.1 ± 3.7	644.7 ± 6.3	1662.8 ± 23.1	25/16
200 GeV	0–10%	39159.617 ± 4620.834	12.898 ± 1.187	0.003 ± 0.001	270.1 ± 3.4	632.1 ± 5.6	1679.6 ± 19.3	28/17
	10–20%	26932.924 ± 4228.469	12.275 ± 1.522	0.004 ± 0.001	270.1 ± 4.6	625.8 ± 8.1	1614.2 ± 24.2	47/17
	20–30%	15241.632 ± 1950.929	32.015 ± 3.130	0.008 ± 0.001	267.8 ± 4.0	540.0 ± 5.5	1405.5 ± 15.6	25/16
	30–40%	21424.977 ± 2067.510	38.813 ± 3.027	0.015 ± 0.001	245.0 ± 3.7	514.1 ± 4.1	1287.1 ± 9.5	17/16
	40–50%	9237.099 ± 715.875	25.366 ± 1.700	0.011 ± 0.001	257.8 ± 2.3	514.1 ± 3.2	1261.9 ± 8.7	13/15
	50–60%	5590.671 ± 768.158	13.275 ± 1.147	0.003 ± 0.001	247.0 ± 4.2	523.5 ± 4.9	1391.6 ± 14.6	25/15
	60–70%	4166.770 ± 475.012	15.232 ± 1.226	0.008 ± 0.001	241.8 ± 3.4	487.9 ± 4.2	1150.6 ± 10.0	13/14
	70–80%	1619.227 ± 182.973	8.987 ± 0.681	0.011 ± 0.001	243.9 ± 3.4	478.3 ± 4.1	999.4 ± 7.1	13/13
	80–92%	847.819 ± 92.412	3.985 ± 0.327	0.005 ± 0.001	234.0 ± 3.2	464.0 ± 3.8	979.4 ± 8.1	16/13
Figure 2	200 GeV	19489.150 ± 2436.144	23.238 ± 3.044	0.010 ± 0.001	255.0 ± 5.1	551.0 ± 7.2	1357.3 ± 12.2	29/18
Cu-Cu 0–10%	62.4 GeV	16881.004 ± 2886.652	16.101 ± 2.505	–	234.3 ± 5.2	475.0 ± 6.7	–	36/8
Figure 3	200 GeV	239.849 ± 52.287	0.128 ± 0.026	0.000022 ± 0.000004	211.0 ± 8.0	534.9 ± 9.5	1398.2 ± 28.0	85/19
<i>pp</i>	62.4 GeV	204.263 ± 59.233	0.030 ± 0.006	–	199.9 ± 7.8	492.7 ± 8.8	–	108/8

to Cu-Cu collisions for V_2 , it does not affect obviously the tendency of volume parameter which is mainly determined by V_1 . Generally, V_1 and T_1 , which determine the volume and temperature of the system respectively, decrease with the decrease of nuclear size.

From the first generation strings to the third ones, the collision system expands rapidly from the volume V_3 to V_2 and then to V_1 . It is expected that the number of the third generation strings is very large, which results in very large volume at the final kinetic freeze-out stage. We believe that the first generation strings are produced earlier than the second ones, and the second ones are produced earlier than the third ones. This renders the volume order of $V_3 < V_2 < V_1$ and the temperature order of $T_3 > T_2 > T_1$, which reflects the volume and temperature dynamics of the system evolution.

At 62.4 GeV, only two generation strings are needed and smaller parameters are obtained. It is expected that single generation strings are suitable to fit the p_T spectra at lower energy, though the single generation strings may exist for a considerable time. At higher energy, it is expected that four or more generation strings can appear. Generally, in relativistic collisions, the string breaking and hadronization depend on energy of the collision, no matter how fast the projectile and target passes through each other.

It should be noted that the temperature parameters T_i extracted from this work contains the influence of collective flow which results in T_i being larger than the kinetic freeze-out temperature T_0 . As discussed in Section 1, one has a few methods to extract T_0 and the transverse flow velocity $\langle\beta_T\rangle$. Based on these methods, there are many works [5, 6, 7, 8, 13, 14, 15, 16] which studied the extractions of T_0 and $\langle\beta_T\rangle$. Although the main focus of this work is on a simple and useful method for studying the fine multi-region structure of the p_T spectra, we may use an almost model-independent approach to extract T_0 and $\langle\beta_T\rangle$.

According to ref. [60], one has the relation, $\langle p_T \rangle =$

$3.07T_0$. Then, we have the almost model-independent $T_0 = \langle p_T \rangle / 3.07$ and $\langle\beta_T\rangle = (2.07/3.07)\langle p_T \rangle / \langle m \rangle$. One can see that T_0 and $\langle\beta_T\rangle$ depends mainly on $\langle p_T \rangle$ and $\langle m \rangle$ which originate from the data, but not from the model. However, the factor 3.07 in this approach comes from the model [60]. Therefore, we say this approach being the almost model-independent. In the case of applying the string model phenomenology, a string is formed by the interaction of two partons via exchange of virtual gluons. For each parton, we should use $\langle p_T \rangle / 2$ instead of $\langle p_T \rangle$ in the expressions of T_0 and $\langle\beta_T\rangle$. At the same time, $\langle m \rangle$ is the constituent mass (0.31 GeV/c [61]) of up or down quarks multiplied by the average Lorentz factor $\langle\gamma\rangle$, where $\langle\gamma\rangle \approx 6$ from the average energy [18] of pions in the rest frame of emission source at the RHIC. Here, we have used the method for calculating the average energy of particles in the source rest frame discussed in collisions at higher energy [18].

Based on the discussion of the almost model-independent T_0 and $\langle\beta_T\rangle$, our calculations show that T_0 approximately equals to 122–109 MeV and $\langle\beta_T\rangle$ approximately equals to 0.135–0.122 c from central to peripheral Au-Au collisions. Meanwhile, $T_0 \approx 118$ and 106 MeV, $\langle\beta_T\rangle \approx 0.131$ and 0.118 c , for central Cu-Cu collisions at 200 and 62.4 GeV respectively; $T_0 \approx 97$ and 91 MeV, $\langle\beta_T\rangle \approx 0.108$ and 0.101 c , for pp collisions at 200 and 62.4 GeV respectively. These results are based on a comprehensive analysis for three- or two-component in the p_T range from 0 to 30 GeV/c and show that T_0 and $\langle\beta_T\rangle$ decrease with the decrease of centrality, nuclear size, and collision energy.

To study the T_0 and $\langle\beta_T\rangle$ dynamics of the system evolution in detail, we now calculate T_{0i} and $\langle\beta_T\rangle_i$ which are the kinetic freeze-out temperature and average transverse flow velocity of the i -th component respectively. In the calculation of the i -th component, the contributions of other components are excluded. Table 2 shows the values of extracted parameters T_{01} , T_{02} , T_{03} , $\langle\beta_T\rangle_1$, $\langle\beta_T\rangle_2$, and $\langle\beta_T\rangle_3$ corresponding to the solid

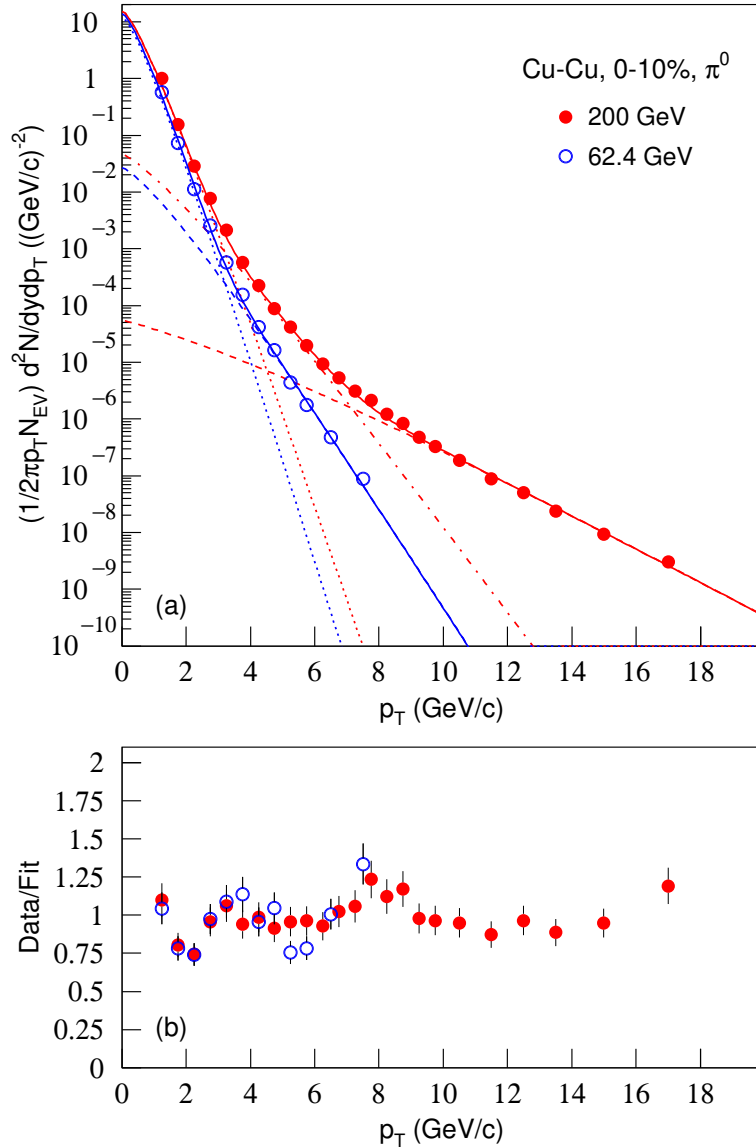


Fig. 2. (a) The invariant yields, $(1/2\pi p_T N_{EV})d^2N/dydp_T$, of π^0 produced in $|\eta| < 0.35$ in 0–10% Cu-Cu collisions at $\sqrt{s_{NN}} = 200$ and 62.4 GeV. The symbols represent the experimental data measured by the PHENIX Collaboration [59]. The curves are our fits by the multi-component standard distribution, Eqs. (1) and (7). (b) Values of Data/Fit corresponding to the fits in panel (a).

curves in Figures 1–3. To present the tendencies of the kinetic freeze-out parameters on centrality intuitively, these values are also displayed in Figures 6 and 7, where the latter is in terms of relative values as Figure 5.

From Figures 6 and 7, one can see that T_{03} and $\langle\beta_T\rangle_3$ decrease significantly, T_{02} and $\langle\beta_T\rangle_2$ decrease slightly, and T_{01} and $\langle\beta_T\rangle_1$ almost do not change with the decrease of centrality from central to peripheral collisions. Meanwhile, the relative values of $T_{03,02}$ and $\langle\beta_T\rangle_{3,2}$ decrease significantly, and the relative values of T_{01} and $\langle\beta_T\rangle_1$ decrease slightly. The tendencies of relative T_{0i} and $\langle\beta_T\rangle_i$ are the same as that of relative T_i shown in Figure 5(b), but different from that of relative V_i shown in Figure 5(a). The consistent results for relative T_i , T_{0i} ,

and $\langle\beta_T\rangle_i$ are understandable, because all three reflect $\langle p_T \rangle$. They are different from relative V_i which reflects the yields or normalization.

In higher energy collisions at the Large Hadron Collider, if the range of p_T spectra is wide enough, the multi-region structure of p_T spectra is usually observed [21, 22, 23]. The multi-component standard distribution in the framework of multi-source thermal model should describe the multi-region structure naturally, where the number of components may be large enough. Although lots of parameters are needed in the case of multi-component, the physics explanation is acceptable due to the multi-source of particles and multi-generations of strings in the complex collisions. In lower

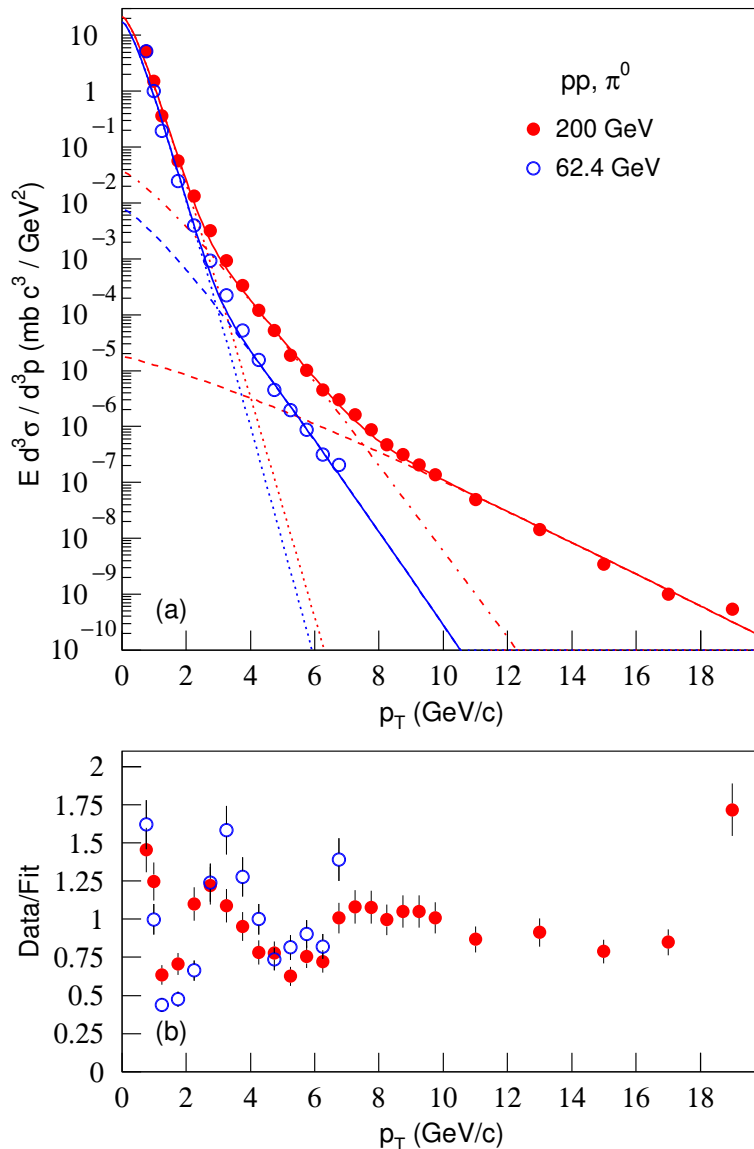


Fig. 3. (a) The invariant cross-sections, $E d^3\sigma / d^3p$, of π^0 produced in $|\eta| < 0.35$ in pp collisions at $\sqrt{s_{NN}} = 200$ and 62.4 GeV. The symbols represent the experimental data measured by the PHENIX Collaboration [59]. The curves are our fits by the multi-component standard distribution, Eqs. (1) and (7). (b) Values of Data/Fit corresponding to the fits in panel (a).

energy collisions at a few GeV, if the range of p_T spectra is not too wide, a two-component standard distribution is suitable, where the first component describes the soft process and the second component describes the hard process. If $T_1 \approx T_2$, a sole component is approximately applicable.

The interpretation of the results in terms of generations of strings seems not satisfactory at very low collision energies, though at which we may consider alternatively the formation of nucleon clusters in the system, if the generations of strings are not available. Meanwhile, the number of components may be 2 or even 1, which is the special cases of the multi-source. In our opinion, the multi-source thermal model can be used by experimen-

tal collaborations to describe and extrapolate the data on multi-particle productions at low and high energies. We believe that the picture of multi-source is suitable for various collisions, though the physics interpretations on sources themselves may be different at different energies.

We would like to point out that although other functions such as the Tsallis and q -dual distributions can fit the p_T spectra by fewer parameters [32, 33, 34, 35, 50, 56], they covered up the fine multi-region structure of the p_T spectra. To study the volume, temperature, and flow velocity dynamics of the system evolution in the framework of multi-source thermal model [24, 25, 26, 27], we are inclined to the multi-component standard

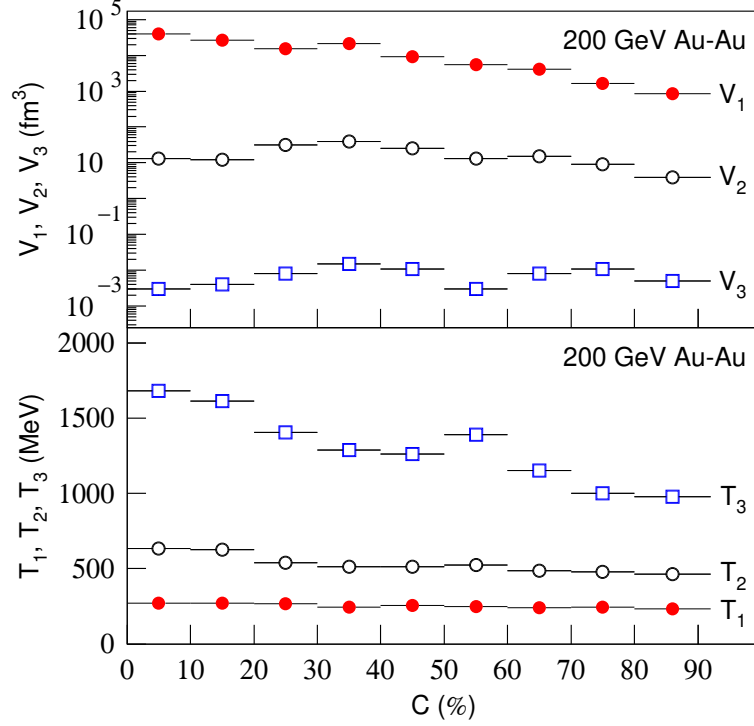


Fig. 4. Dependences of normalization constants V_1 , V_2 , and V_3 (upper panel), as well as free parameters T_1 , T_2 , and T_3 (lower panel), on the centrality C in 200 GeV Au-Au collisions. Different symbols represent different parameters marked in the panels.

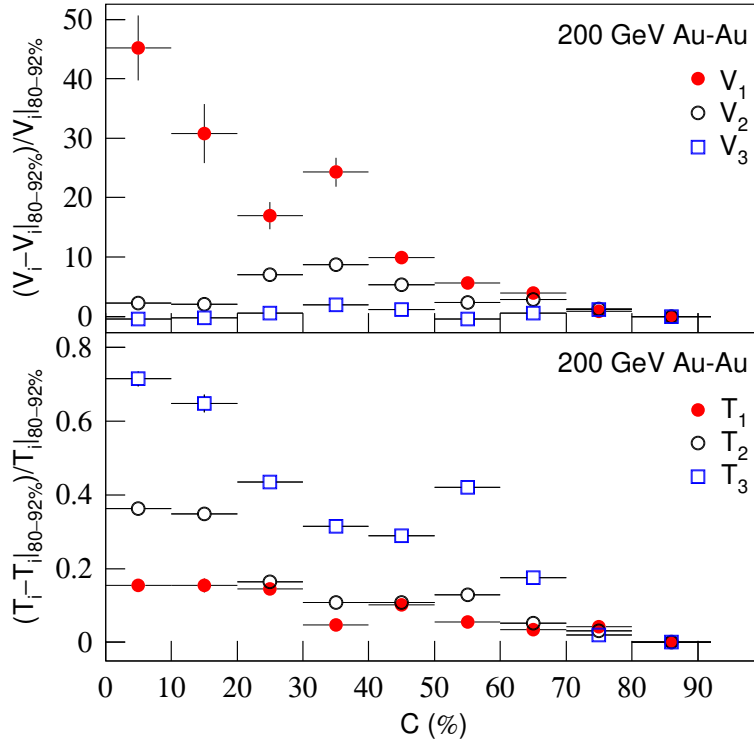


Fig. 5. Dependences of $(V_i - V_i|_{80-92\%})/V_i|_{90-92\%}$ (upper panel) and $(T_i - T_i|_{80-92\%})/T_i|_{90-92\%}$ (lower panel) on C in 200 GeV Au-Au collisions. Different symbols represent different parameters marked in the panels.

distribution which is also the most classic distribution and “thermometer” in the ideal gas model in thermo-

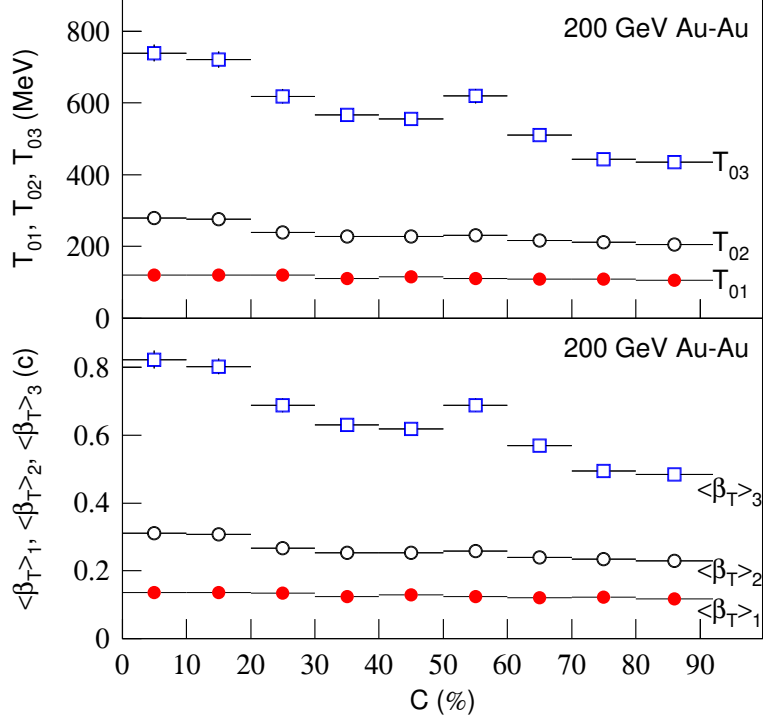


Fig. 6. Dependences of extracted parameters T_{01} , T_{02} , and T_{03} (upper panel), as well as $\langle\beta_T\rangle_1$, $\langle\beta_T\rangle_2$, and $\langle\beta_T\rangle_3$ (lower panel), on the centrality C in 200 GeV Au-Au collisions. Different symbols represent different parameters marked in the panels.

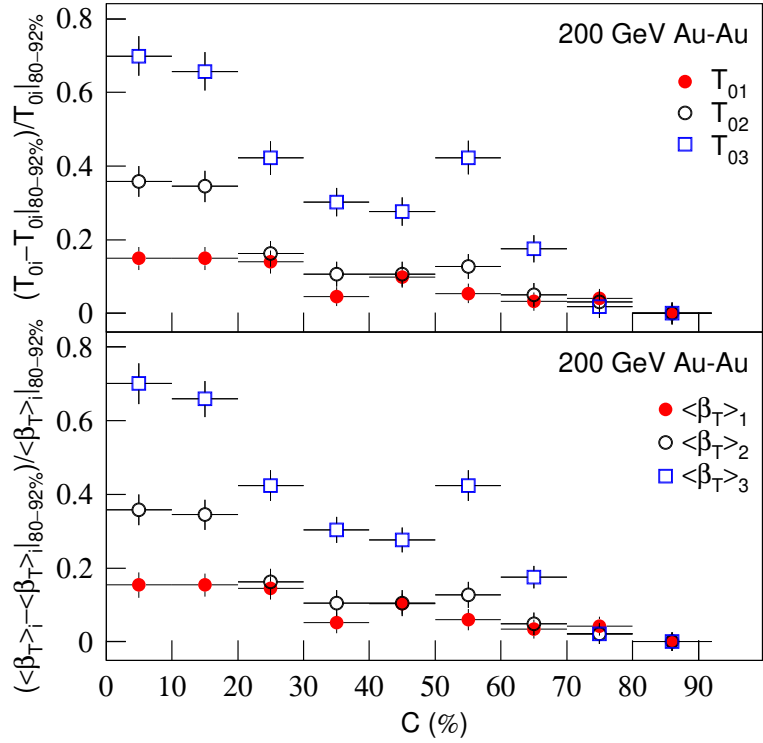


Fig. 7. Dependences of $(T_{0i} - T_{0i}|_{80-92\%})/T_{0i}|_{90-92\%}$ (upper panel) and $(\langle\beta_T\rangle_i - \langle\beta_T\rangle_i|_{80-92\%})/\langle\beta_T\rangle_i|_{90-92\%}$ (lower panel) on C in 200 GeV Au-Au collisions. Different symbols represent different parameters marked in the panels.

dynamics. Usually, the standard-thermometer obtains higher temperature than the Tsallis-thermometer [62].

Table 2. Values of extracted parameters T_{01} , T_{02} , T_{03} , $\langle\beta_T\rangle_1$, $\langle\beta_T\rangle_2$, and $\langle\beta_T\rangle_3$ corresponding to the solid curves in Figures 1–3.

Figure	Selection	T_{01} (MeV)	T_{02} (MeV)	T_{03} (MeV)	$\langle\beta_T\rangle_1$ (c)	$\langle\beta_T\rangle_2$ (c)	$\langle\beta_T\rangle_3$ (c)
Figure 1	0–100%	115.4 ± 3.0	241.2 ± 7.2	638.1 ± 21.2	0.128 ± 0.003	0.268 ± 0.008	0.710 ± 0.022
Au-Au	0–5%	121.0 ± 3.3	284.7 ± 8.8	732.0 ± 22.9	0.135 ± 0.003	0.317 ± 0.010	0.815 ± 0.025
200 GeV	0–10%	121.0 ± 3.3	279.1 ± 8.5	739.3 ± 23.4	0.135 ± 0.004	0.311 ± 0.010	0.823 ± 0.027
	10–20%	121.0 ± 3.3	276.4 ± 8.7	721.2 ± 22.6	0.135 ± 0.004	0.308 ± 0.009	0.803 ± 0.024
	20–30%	120.0 ± 3.2	238.8 ± 7.1	618.9 ± 20.0	0.134 ± 0.004	0.266 ± 0.008	0.689 ± 0.020
	30–40%	110.1 ± 2.7	227.4 ± 6.9	566.8 ± 16.8	0.123 ± 0.003	0.253 ± 0.008	0.631 ± 0.017
	40–50%	115.7 ± 3.0	227.4 ± 6.9	555.7 ± 16.6	0.129 ± 0.003	0.253 ± 0.008	0.618 ± 0.016
	50–60%	111.0 ± 2.7	231.6 ± 7.0	619.2 ± 20.0	0.124 ± 0.003	0.258 ± 0.008	0.689 ± 0.020
	60–70%	108.7 ± 2.7	216.0 ± 6.6	511.3 ± 16.0	0.121 ± 0.003	0.240 ± 0.007	0.569 ± 0.015
	70–80%	109.6 ± 2.7	211.8 ± 6.4	443.5 ± 13.4	0.122 ± 0.003	0.234 ± 0.006	0.494 ± 0.013
	80–92%	105.3 ± 2.6	205.5 ± 6.2	435.2 ± 13.2	0.117 ± 0.002	0.229 ± 0.006	0.484 ± 0.012
Figure 2	200 GeV	116.3 ± 3.0	243.4 ± 7.4	597.4 ± 18.3	0.129 ± 0.003	0.271 ± 0.009	0.665 ± 0.019
Cu-Cu 0–10%	62.4 GeV	105.1 ± 2.6	210.1 ± 6.3	–	0.117 ± 0.003	0.234 ± 0.006	–
Figure 3	200 GeV	95.1 ± 2.4	236.3 ± 7.0	615.4 ± 19.9	0.106 ± 0.002	0.263 ± 0.008	0.685 ± 0.020
<i>pp</i>	62.4 GeV	90.3 ± 2.3	217.8 ± 6.6	–	0.100 ± 0.003	0.242 ± 0.007	–

Using the multi-source thermal model to describe emission from the different stages of the system evolution looks like an approximation to a more dynamic one, like a well-know hydrodynamic model [63, 64, 65]. However, in a hydrodynamic model, there is typically one freeze-out temperature and a distribution of flow velocities on the freeze-out surface (surface of constant temperature) with which hadrons are produced. The present work treats the system evolution at different stages by different temperature and flow velocities.

Indeed, the approach used in the present work is different from the widely used hydrodynamic one in some ways. According to the hydrodynamic models, one freeze-out temperature can describe the p_T range only up to 3 GeV/ c . Anything above that is typically assumed to be non-thermal. However, in our opinion, the two types of treatments may be consistent if one considers a multi-component hydrodynamic model in which two or three sets of parameters may be used. Of course, one may have different explanations for the second and third components in the thermal and hydrodynamic descriptions.

In addition, the present work just uses the thermal description for particle productions based on the generations of strings in general parton’s interactions, but not the jet productions due to head on parton’s collisions. At the string or parton level, one can see that the highest kinetic freeze-out temperature (T_{03}) reaches up to above 700 MeV for high- p_T (~ 16 GeV/ c) particle productions in central Au-Au collisions at the RHIC. Although this temperature is very high and its contribution range is very wide, its fraction is very low. Combining with low- p_T particles, the temperature is only ~ 120 MeV which is less than the well-know chemical freeze-out temperature (~ 150 – 160 MeV [51, 52, 53, 54]).

Before summarizing and conclusions, it should be noted that the present work studies V_i dynamics which is different from the volume obtained using the correlations method [66]. In the latter, the pion source radii obtained from the two-pion Bose-Einstein correlation functions in central Pb-Pb collisions at 2.76 TeV to be similar to the nuclear size. The present work obtained the source volume to increase quickly from the parton size (V_3) to the volume of an expanding fireball (V_1) which is much larger than the nuclear size. As mentioned in the last section, we have $k_i = V_i / \sum V_i$. This results in $k_1 > 99.5\% - 99.9\%$ from Table 1. The parameters from the first component can represent the ones from the average weighted k_i over the multiple components. In addition, V_3 is very small. To show V_3 appropriately, V_1 and V_2 are showed by high precise uncertainties so that three V_i have the same number of decimal places.

4 Conclusions

In the framework of multi-source thermal model, we have studied the fine multi-region structure of the transverse momentum spectra of π^0 produced in mid-rapidity region in Au-Au, Cu-Cu, and *pp* collisions at the RHIC. We are inclined to the multi-component standard distribution which can be used to extract the parameters for the fine structure of the spectra since it is the most classical distribution in the ideal gas model, though other functions such as the Tsallis and q -dual distributions can fit the spectra by fewer parameters. In this work, the temperature and flow effect is separated by an alternative method which is almost model-independent.

The significance of the present work is in the methodology, though it is a simple application of the multi-

component standard distribution. The success of this work reflects that the classical theory can still play a great role in the field of relativistic collisions. In nucleus-nucleus collisions, the volume, temperature, and flow velocity parameters decrease with the decrease of centrality from central to peripheral collisions. These parameters also decrease with the decrease of nuclear size and collision energy. It is natural that at lower (higher) energy, fewer (more) components of the distribution or generations of the strings are needed.

Combining with the string model phenomenology, in the case of using the three-component standard distribution, we could conjecture that the high-temperature term corresponds to the hadronization of the first generation strings, and the intermediate- and low-temperature terms correspond to the hadronization of the second and third generation strings respectively. The third generation strings are from the breaking of the second generation strings, and the second generation strings are from the breaking of the first generation strings.

From the first generation strings to the third ones, the increasing volume parameter and the decreasing temperature (flow velocity) parameter describe the volume and temperature (flow velocity) dynamics of the system evolution respectively. Obtained V_i and T_i , $i = 1$ to 3 values, see Table 1, indicate a rapid expansion of the system, which gradually cools down, causing the particle velocity to decrease, see Table 2. Expecting the formation of the first generation of strings to happen during the initial stage of the relativistic collisions, the highest temperature (T_{03} , see Table 2) could be attributed to the initial temperature of the system at the string or parton level.

Acknowledgements The authors would like to thank the anonymous reviewer for his/her many constructive comments. The work of Shanxi Group was supported by the National Natural Science Foundation of China under Grant No. 12147215, the Shanxi Provincial Natural Science Foundation under Grant No. 202103021224036, and the Fund for Shanxi “1331 Project” Key Subjects Construction. The work of K.K.O. was supported by the Agency of Innovative Development under the Ministry of Higher Education, Science and Innovations of the Republic of Uzbekistan within the fundamental project No. F3-20200929146 on analysis of open data on heavy-ion collisions at RHIC and LHC.

Data Availability Statement The data used to support the findings of this study are included within the article and are cited at relevant places within the text as references.

Declarations

Conflicts of Interest The authors declare that there are no conflicts of interest regarding the publication of this paper. The funding agencies have no role in the design of the study; in the collection, analysis, or interpretation of the data; in the writing of the manuscript; or in the decision to publish the results.

References

- [1] A N Tawfik, M Hanafy and W Scheinast *Indian J. Phys.* **96** 2993 (2022)
- [2] Y Su, X L Chen, Y J Sun and Y F Zhang *Nucl. Sci. Tech.* **32** 108 (2021)
- [3] I Khan, M Iqbal, A Zaman and N Ullah *Indian J. Phys.* **96** 1259 (2022)
- [4] M Ghimiray, N Subba, A Ahmed, A N Tawfik and P K Haldar *Indian J. Phys.* **97** 1551 (2023)
- [5] E Schnedermann, J Sollfrank and U Heinz *Phys. Rev. C* **48** 2462 (1993)
- [6] B I Abelev, M M Aggarwal, Z Ahammed et al. [STAR Collaboration] *Phys. Rev. C* **79** 034909 (2009)
- [7] B I Abelev, M M Aggarwal, Z Ahammed et al. [STAR Collaboration] *Phys. Rev. C* **81** 024911 (2010)
- [8] Z B Tang, Y C Xu, L J Ruan, G van Buren, F Q Wang and Z B Xu *Phys. Rev. C* **79** 051901(R) (2009)
- [9] J Cleymans and D Worku *Eur. Phys. J. A* **48** 160 (2012)
- [10] P K Khandai, P Sett, P Shukla and V Singh *J. Phys. G* **41** 025105 (2014)
- [11] K K Olimov, S Z Kanokova, K Olimov et al. *Mod. Phys. Lett. A* **35** 2050115 (2020)
- [12] K K Olimov, S Z Kanokova, A K Olimov et al. *Mod. Phys. Lett. A* **35** 2050237 (2020)
- [13] K K Olimov, A Iqbal and S Masood *Int. J. Mod. Phys. A* **35** 2050167 (2020)
- [14] H Heiselberg and A-M Levy *Phys. Rev. C* **59** 2716 (1999)
- [15] U W Heinz *2003 CERN-CLAF School of High-Energy Physics* (San Miguel Regla, Mexico, 2003) (ed) N Ellis (Switzerland: CERN Yellow Report) p 165 (2006), arXiv:hep-ph/0407360 (2004)
- [16] S Takeuchi, K Murase, T Hirano, P Huovinen and Y Nara *Phys. Rev. C* **92** 044907 (2015)
- [17] R Russo *PhD thesis* (Universita degli Studi di Torino, Italy) (2015), arXiv:1511.04380 [nucl-ex] (2015)
- [18] H-L Lao, H-R Wei, F-H Liu and R A Lacey *Eur. Phys. J. A* **52** 203 (2016)
- [19] A Khatun, D Thakur, S Deb and R Sahoo *J. Phys. G* **47** 055110 (2020)
- [20] D Sahu, S Tripathy, G S Pradhan and R Sahoo *Phys. Rev. C* **101** 014902 (2020)
- [21] M Suleymanov *Int. J. Mod. Phys. E* **27** 1850008 (2018)
- [22] M Suleymanov *Int. J. Mod. Phys. E* **28** 1950084 (2019)
- [23] M Suleymanov, arXiv:2102.00440 [hep-ph] (2021)
- [24] F-H Liu *Nucl. Phys. A* **810** 159 (2008)
- [25] F-H Liu and J-S Li *Phys. Rev. C* **78** 044602 (2008)
- [26] F-H Liu *Phys. Rev. C* **78** 014902 (2008)

- [27] F-H Liu, B K Singh and N N Abd Allah *Proceedings of the 14th International Symposium on Very High Energy Cosmic Ray Interactions* (Weihai, China, 2006) (Nucl. Phys. B (Proc. Suppl.) 175–176) (eds) K S Cheng, R Engel, Y Q Ma, B Pattison, Z G Yao and Q Q Zhu (The Netherlands: Elsevier Press) p 54 (2008)
- [28] R Hagedorn *Riv. Nuovo Cim.* **6**(10) 1 (1983)
- [29] B Abelev, J Adam, D Adamová et al. [ALICE Collaboration] *Eur. Phys. J. C* **75** 1 (2015)
- [30] K Aamodt, N Abel, U Abeyssekara et al. [ALICE Collaboration] *Phys. Lett. B* **693** 53 (2010)
- [31] A De Falco [for the ALICE Collaboration] *J. Phys. G* **38** 124083 (2011)
- [32] C Tsallis *J. Stat. Phys.* **52** 479 (1988)
- [33] C Tsallis *Braz. J. Phys.* **39** 337 (2009)
- [34] T S Biró, G Purcsel and K Urmössy *Eur. Phys. J. A* **40** 325 (2009)
- [35] J Cleymans and M W Paradza *Physics* **2** 654 (2020)
- [36] E K G Sarkisyan and A S Sakharov *The 35th International Symposium on Multiparticle Dynamics (ISMD 05) and 1st Workshop on Particle Correlations and Femtoscopy (WPCF 2005)* (Kromeriz, Czech Republic, 2005) (AIP Conf. Proc. 828) (eds) V Simak, M Sumera, S Todorova-Nova and B Tomasik (New York: AIP) p 35 (2006)
- [37] E K G Sarkisyan and A S Sakharov *Eur. Phys. J. C* **70** 533 (2010)
- [38] A N Mishra, R Sahoo, E K G Sarkisyan and A S Sakharov *Eur. Phys. J. C* **74** 3147 (2014) and Erratum *Eur. Phys. J. C* **75** 70 (2015)
- [39] E K G Sarkisyan, A N Mishra, R Sahoo and A S Sakharov *Phys. Rev. D* **93** 054046 (2016) and Erratum *Phys. Rev. D* **93** 079904 (2016)
- [40] E K G Sarkisyan, A N Mishra, R Sahoo and A S Sakharov *Phys. Rev. D* **94** 011501(R) (2016)
- [41] E K G Sarkisyan, A N Mishra, R Sahoo and A S Sakharov *EPL (Europhys. Lett.)* **127** 62001 (2019)
- [42] A N Mishra, A Ortiz and G Paic *Phys. Rev. C* **99** 034911 (2019)
- [43] P Castorina, A Iorio, D Lanteri, H Satz and M Spusta *Phys. Rev. C* **101** 054902 (2020)
- [44] K Werner *Phys. Rep.* **232** 87 (1993)
- [45] A M Badalian, V D Orlovsky and Y A Simonov *Phys. Atom. Nucl.* **76** 955 (2013)
- [46] Y A Simonov *Phys. Rev. D* **84** 065013 (2011)
- [47] S C Frautschi *Phys. Rev. D* **3** 2821 (1971)
- [48] F Csikor, Z Katona and I Montvay *Lett. Nuovo Cim.* **8** 99 (1973)
- [49] H Satz *Phys. Rev. D* **19** 1912 (1979)
- [50] A S Parvan *Eur. Phys. J. A* **56** 106 (2020)
- [51] A Andronic, P Braun-Munzinger and J Stachel *Nucl. Phys. A* **772** 167 (2006)
- [52] A Andronic, P Braun-Munzinger and J Stachel *Acta Phys. Pol. B* **40** 1005 (2009)
- [53] A Andronic, P Braun-Munzinger and J Stachel *Nucl. Phys. A* **834** 237c (2010)
- [54] A Andronic, P Braun-Munzinger, K Redlich and J Stachel *Nature* **561** 321 (2018)
- [55] H-X Zhang and P-J Shan, *Statistical simulation method for determinating the errors of fit parameters*, in Proc. 8th Natl. Conf. Nucl. Phys. (Volume II), Xi'an, China (December 1991)
- [56] F-H Liu, Y-Q Gao and H-R Wei *Adv. High Energy Phys.* **2014** 293873 (2014)
- [57] N Yu and X-F Luo, *Eur. Phys. J. A* **55** 26 (2019)
- [58] A Adare, S Afanasiev, C Aidala et al. [PHENIX Collaboration] *Phys. Rev. Lett.* **101** 232301 (2008)
- [59] A Adare, S Afanasiev, C Aidala et al. [PHENIX Collaboration] *Phys. Rev. Lett.* **101** 162301 (2008)
- [60] G Giacalone *PhD thesis* (Université Paris-Saclay, France) (2021), arXiv:2101.00168 [nucl-th] (2021)
- [61] Z-J Xiao and C-D Lü *Introduction to Particle Physics* (Beijing, China: Science Press) Ch 6, Sec 2, p 160 (2016)
- [62] G Biró, G G Barnaföldi and T S Biró, arXiv:2003.03278 [hep-ph] (2020)
- [63] C Gale, S Jeon and B Schenke *Int. J. Mod. Phys. A* **28** 1340011 (2013)
- [64] A Jaiswal and V Roy *Adv. High Energy Phys.* **2016** 9623034 (2016)
- [65] C Shen and L Yan *Nucl. Sci. Tech.* **31** 122 (2020)
- [66] K Aamodt, A A Quintana, D Adamová et al. [ALICE Collaboration] *Phys. Lett. B* **696** 328 (2011)